Biosensors and Bioelectronics 261 (2024) 116472

Contents lists available at ScienceDirect

Biosensors and Bioelectronics

journal homepage: www.elsevier.com/locate/bios

Recent advances in soft, implantable electronics for dynamic organs

Won Bae Han [a,b,c,1], Tae-Min Jang [c,1], Beomjune Shin [a,b,1], Venkata Ramesh Naganaboina [c,1], Woon-Hong Yeo [a,b,d,e], Suk-Won Hwang [c,f,g,*]

[a] George W. Woodruff School of Mechanical Engineering, Georgia Institute of Technology, Atlanta, GA, 30332, USA
[b] IEN Center for Wearable Intelligent Systems and Healthcare, Georgia Institute of Technology, Atlanta, GA, 30332, USA
[c] KU-KIST Graduate School of Converging Science and Technology, Korea University, Seoul, 02841, Republic of Korea
[d] Wallace H. Coulter Department of Biomedical Engineering, Georgia Tech and Emory University School of Medicine, Atlanta, GA, 30332, USA
[e] Parker H. Petit Institute for Bioengineering and Biosciences, Institute for Materials, Institute for Robotics and Intelligent Machines, Georgia Institute of Technology, Atlanta, GA, 30332, USA
[f] Center for Biomaterials, Biomedical Research Institute, Korea Institute of Science and Technology (KIST), Seoul, 02792, Republic of Korea
[g] Department of Integrative Energy Engineering, Korea University, Seoul, 02841, Republic of Korea

ARTICLE INFO

Keywords:
Soft material
Implantable electronics
Biomedical application
Bladder-integrated electronics
Cardiac electronics

ABSTRACT

Unlike conventional rigid counterparts, soft and stretchable electronics forms crack- or defect-free conformal interfaces with biological tissues, enabling precise and reliable interventions in diagnosis and treatment of human diseases. Intrinsically soft and elastic materials, and device designs of innovative configurations and structures leads to the emergence of such features, particularly, the mechanical compliance provides seamless integration into continuous movements and deformations of dynamic organs such as the bladder and heart, without disrupting natural physiological functions. This review introduces the development of soft, implantable electronics tailored for dynamic organs, covering various materials, mechanical design strategies, and representative applications for the bladder and heart, and concludes with insights into future directions toward clinically relevant tools.

1. Introduction

Integration of electronic devices with the human body is of importance for precise and timely interventions in diagnostics, therapeutics, and prosthetics. However, established rigid electronics, primarily composed of silicon and metals on stiff substrates, encounter difficulty in interfacing with soft tissues due to several challenges including mechanical mismatch, potential tissue damage and chronic inflammation. When applied to, particularly, dynamic organs undergoing continuous movement and volume fluctuations during normal physiological processes, such electronics would disrupt the deformability, which may lead to discomfort or malfunctions. On the other hand, soft, stretchable counterparts, which revolutionized skin electronics (Chung et al., 2019; Hu et al., 2023; T. T. Kim et al., 2022; Y. Y. Kim et al., 2022; Kwon et al., 2023; S. M. Yang et al., 2022), human-machine interfaces (Kim et al., 2024; Kwon et al., 2020; Tang et al., 2023; Yu et al., 2019), and soft robotics (Baumgartner et al., 2020; Byun et al., 2018; Kim et al., 2021; Mao et al., 2022; M. H. Oh et al., 2023), can offer seamless integration with biological tissues, thanks to their mechanical compliance achieved through materials engineering and structural designs. Various elastomeric polymers with low moduli responded to external strains, serving as soft, elastic substrates (Han et al., 2023b; Li et al., 2023; Maeng et al., 2020; Shin et al., 2024; Wang et al., 2018), while conductive polymer composites, hydrogels, and liquid metals maintained electrical conductivity across a wide range of strain and are utilized as intrinsically stretchable electrodes (Bartlett et al., 2017; Choi et al., 2018; Han et al., 2022; Ohm et al., 2021; Zhou et al., 2023; Zhuang et al., 2023). Moreover, innovative mechanical designs through mesh structures, island-bridge configurations, fractal layouts, and modulus-gradient structures significantly reduced modulus mismatch at the device-tissue interface (Ausra et al., 2022; Bandodkar et al., 2017; Fan et al., 2014; Han et al., 2023b; Wonho Lee et al., 2018; Li et al., 2023). These advancements facilitate reliable, long-term monitoring and treatment of diverse diseases, enabling clinically relevant applications such as drug delivery (Kaveti et al., 2024; Koo et al., 2020), tissue regeneration (Choi et al., 2020; Koo et al., 2018; L. Wang et al., 2022; Wang et al., 2020),

* Corresponding author. KU-KIST Graduate School of Converging Science and Technology, Korea University, Seoul, 02841, Republic of Korea.
E-mail address: dupong76@korea.ac.kr (S.-W. Hwang).
[1] Won Bae Han, Tae-Min Jang, Beomjune Shin, and Venkata Ramesh Naganaboina contributed equally to this work.

https://doi.org/10.1016/j.bios.2024.116472
Received 31 March 2024; Received in revised form 29 May 2024; Accepted 5 June 2024
Available online 6 June 2024

neuromodulation (Lee et al., 2023; Liu et al., 2020; Mickle et al., 2019), and pacemaking (Choi et al., 2021, 2022; Sim et al., 2020).

In this review, we comprehensively explore materials and device structures tailored for soft, implantable electronics, with a particular focus on dynamic organs like bladder and heart. Beginning with a discussion of mechanically compliant and soft electronic materials, the review then delves into mechanical design methodologies aimed at mitigating mechanical mismatch at the device-tissue interface to achieve conformal contact and high signal-to-noise ratios. Subsequently, representative applications in real-time diagnostics and therapeutic functions for the bladder and heart are briefly discussed, and concluding remarks provide insights into the current landscape and future prospects of soft, implantable electronics for successful clinical translation of these innovative technologies.

2. Materials for soft, implantable electronics

Electronic components or systems have been dominated by rigid materials such as silicon and ceramics, which offers excellent electrical properties and high-quality long-term biointerfaces although the mechanical rigidity poses limitations (Koo et al., 2021; Shim et al., 2021; Zhang et al., 2023): (i) they cannot adapt to fit smoothly against non-flat biological surfaces, and (ii) immune reactions and persistent inflammation, unsuitable for long-term internal monitoring and therapy. To complement this technology, significant research efforts have been devoted to development of thin, smooth and curved components, thus mechanically soft, flexible devices and systems attracted considerable attention. The novel mechanical feature of bioelectronics could offer enhanced compatibility with target tissues or organs, thereby enabling high-quality biosensing and effective feedback stimulation in the long run. Addressing this aspect, electronic devices have been designed to be ultrathin with interconnects that were wavy, serpentine, or of a fractal design; the systems incorporated fracture-prone materials near the neutral mechanical plane, enabling to deform and effectively dissipate both tensile and compressive stresses under mechanical deformation (Huang et al., 2019; Yin et al., 2020). Fig. 1a (left) illustrates arrays of functional electronic devices with non-coplanar gold (Au)-based serpentine interconnects, integrated onto a balloon catheter (Kim et al., 2011). The micrograph in Fig. 1a (right) provides a magnified view, showcasing the layout and interconnections of functional systems, including a temperature sensor and an exposed electrocardiogram (EKG) electrode. This study exploited a high-performance balloon catheter platform by incorporating temperature, flow, tactile, and electrophysiological sensors, along with radiofrequency electrodes for controlled, local ablation of tissue with the aim of enhancing the effectiveness of cardiac ablation therapy.

Alongside the unconventional design approaches, soft electronic materials (e.g., intrinsically stretchable conductors) have been developed in recent years to resist potential damages from external deformations (Han et al., 2022; Koo et al., 2021; Park et al., 2016; Sunwoo et al., 2021). Fig. 1b displays a biocompatible, highly conductive (100 mS cm^{-2}) composite consisting of multi-walled carbon nanotube (CNT, length: >100 μm and diameter: 5 nm) sheets dispersed in an aqueous polyrotaxane-based hydrogel (Sekitani et al., 2016). Here, the CNT gel was interconnected with an ultrathin and mechanically flexible organic active-matrix amplifier, which was fabricated on a 1.2-μm thick polyethylene-naphthalate (PEN) film to amplify the epicardial electrocardiography of heart tissue. Fig. 1c (top) demonstrated a bi-continuous conductive polymer hydrogel (BC-CPH), which offered high electrical conductivity (more than 11 S cm^{-1}), fracture toughness (over 3300 J m^{-2}), tissue-like softness (Young's modulus below 1 MPa) and excellent stretchability (over 400%) without sacrificing the mechanical properties (Zhou et al., 2023). BC-CPH was prepared from phase-separated inks consisting of poly(3,4-ethylenedioxythiophene):poly(styrenesulfonate) (PEDOT:PSS) as the electrical phase and hydrophilic polyurethane as the mechanical phase, which exhibited excellent elastic deformation at 200% strain, maintaining the bi-continuous phases without plastic deformation (Fig. 1c, bottom). Interestingly, the prepared inks were amenable to various advanced fabrication methods such as spin-coating, electro-spinning (low-viscosity), micro-moulding and three-dimensional (3D) printing (high-viscosity). For demonstration, they designed 3D printed monolithic all-hydrogel bioelectronic interfaces for electrophysiological recording of the heart and stimulation of the sciatic nerve and spinal cord in rat models. Liquid metal, represented by the eutectic gallium-indium alloy (EGaIn), emerges as a promising conductor for soft, implantable electronics due to its excellent electrical conductivity (~40,000 S cm^{-1}), liquid-state deformability, and negligible toxicity (Zhuang et al., 2023; Guo and Liu, 2017; S. Wang et al., 2022). Fig. 1d represents a schematic illustration of the fabrication process of a high-resolution, super-soft, stretchable, and permeable liquid metal microelectrode (μLME) with a wafer-scale patterning strategy (Zhuang et al., 2023). The fabricated μLMEs provided tissue-like mechanical softness, excellent electrical conductivity even at 1000% strain, long-term skin attachment and biocompatibility, with high resolutions up to 2 μm and ultrahigh density of more than 75,000 electrodes/cm^2 via photolithography. As a proof of concept, a μLME array was designed and deployed at neural interfaces for high-spatiotemporal-resolution mapping and recording of the interference of electrocorticography (ECoG) signals.

The selection of biocompatible and mechanically compliant materials for substrates and encapsulations is a key factor for soft implantable bioelectronics. In this context, a soft electronic dura (e-dura) mater was designed and developed to restore locomotion after spinal cord injury using simultaneous and colocalized electrical and chemical stimulations (Xu et al., 2015). Fig. 1e illustrates a transparent silicone substrate (thickness: 120 μm) containing stretchable gold interconnects (thickness: 35 nm) and electrodes coated with a platinum-silicone alloy (diameter: 300 μm) for transmitting electrical excitations and transferring electrophysiological signals, and a compliant fluid microchannel (cross-section: 100 μm by 50 μm) for drug delivery. Existing stretchable semiconductors and conductors have Young's moduli higher (over 100 MPa) than soft bio-tissues, which limits the tissue-level conformability of the electronic devices (Lacour et al., 2006; Li et al., 2023). Fig. 1f (left) demonstrates the fracture mechanics of thin films supported by elastomeric substrates, where a large modulus difference across the interface intensified stress concentrations at defect sites and increased the rate of coherent energy release under stretching, thus creating a higher tendency for crack propagation. To mitigate this effect, Fig. 1f (middle) presents a novel design strategy for versatile realization of stretchable devices with ultralow tissue-level moduli by allowing a soft interlayer (polystyrene-ethylene-butylene-styrene, SEBS) using an existing elastic material of relatively high moduli (Li et al., 2023). The mechanical tests showed that adding a SEBS interlayer (1.2 μm-thick) to a polyacrylamide (PAAm) hydrogel (200 μm-thick) led to a slight increase in the effective modulus, which was two to three orders of magnitude lower than commonly used elastomeric substrates such as polydimethylsiloxane (PDMS) and SEBS (Fig. 1f, right). Stretchable transistor arrays with moduli below 10 kPa were demonstrated, benefiting from increased conformability to irregular and dynamic surfaces, an ultrasoft device for electrophysiological recording on the isolated heart with high adaptability, spatial stability and minimal impact was realized. In a similar line, mechanically and chemically robust shape programmable materials such as liquid crystal elastomers (LCEs) have been developed for the use of substrates and encapsulations of implantable electronics, and Fig. 1g illustrates synthesis and fabrication procedures of LCEs (Maeng et al., 2020). Helical multichannel cables were fabricated for electrode arrays in programmed 3D shapes, and then stretching and buckling studies were performed over 10,000 cycles at 60% strain when soaked in phosphate-buffered saline (PBS).

Nanocomposite materials have been developed in recent years by incorporating conductive materials into elastomeric media to achieve enhanced stretchability without compromising electrical conductivity.

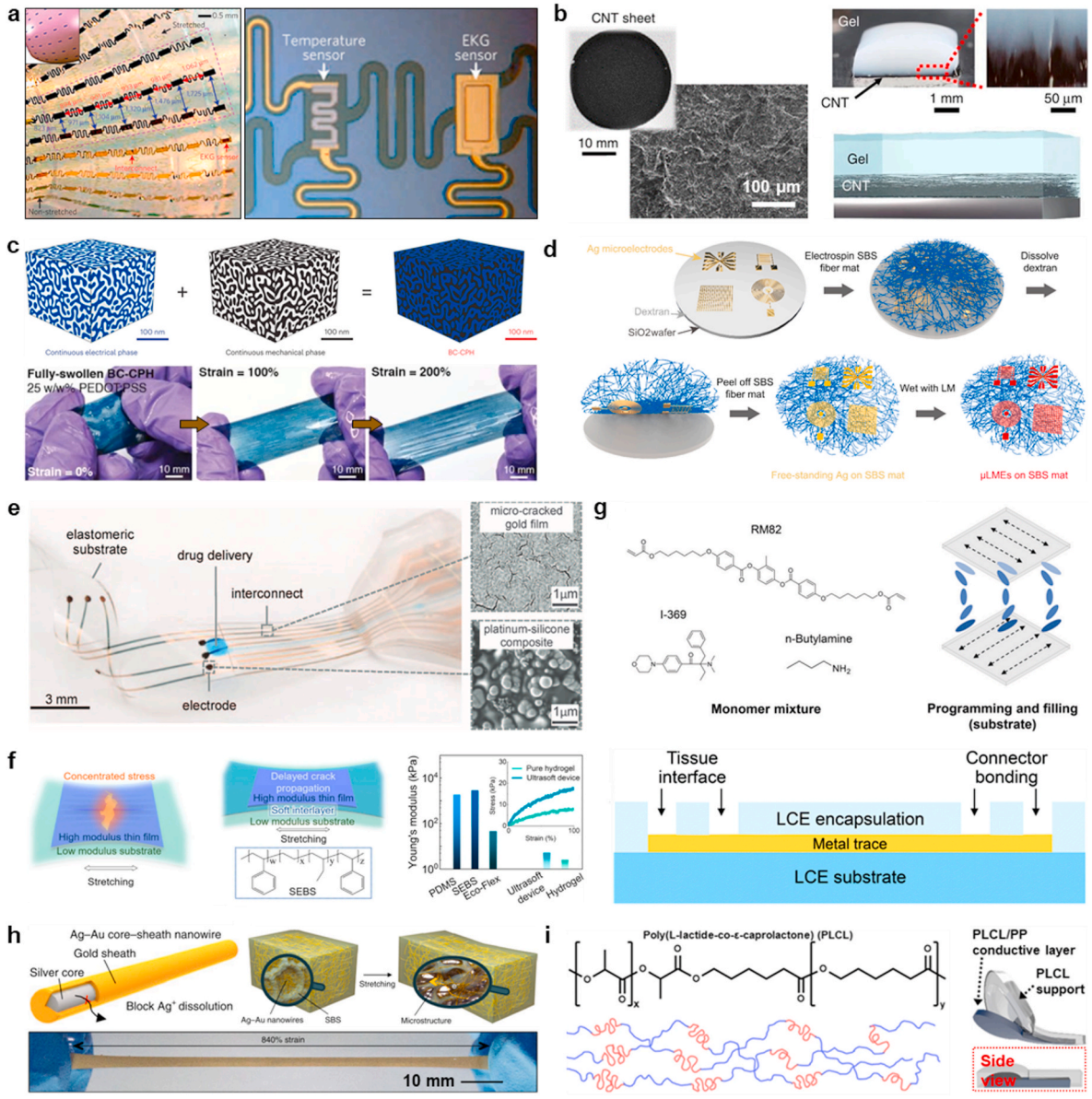

Fig. 1. Material strategies for soft implantable bioelectronics. (a) Integration of stretchable, interconnected passive networks onto a balloon catheter in inflated state (left), and magnified optical image of a temperature sensor and electrodes for electrocardiogram (EKG) (right). Reproduced with permission from (Kim et al., 2011). Copyright 2011, Springer Nature. (b) Conductive carbon nanotube (CNT) sheet and scanning electron microscope (SEM) image (left), and cross-sectional picture (top right) and illustration (bottom right) of the CNT/polyrotaxane composite (Inset shows the magnified picture of the CNT/polyrotaxane interface). Reproduced with permission from (Sekitani et al., 2016). Copyright 2016, Springer Nature. (c) Conceptual overview of a bi-continuous conducting polymer hydrogel (BC-CPH), where PEDOT:PSS and hydrophilic polyurethane (PU) were responsible for the continuous electrical and mechanical phase (top), and sequential images of a fully swollen BC-CPH with 25 w/w% PEDOT:PSS at strains of 0%, 100%, and 200% (bottom). Reproduced with permission from (Zhou et al., 2023). Copyright 2023, Springer Nature. (d) Schematic illustration of the fabrication process of permeable and stretchable liquid metal microelectrodes (μLMEs). Reproduced with permission from (Zhuang et al., 2023). Copyright 2023, AAAS. (e) Optical image of an implantable electronic dura mater (e-dura) for the spinal cord (left), and SEM images of a gold film and platinum-silicone composite (right). Reproduced with permission from (Xu et al., 2015). Copyright 2015, AAAS. (f) Description of stress concentration in an electronic thin film on a substrate with an orders-of-magnitude lower modulus (left), soft-interlayer design using a thin film with an intermediate modulus to reduce the modulus difference at the interface (middle), and Young's modulus of an ultrasoft device built on a polyacrylamide (PAAm) hydrogel substrate with different soft interlayers (right, inset shows the strain-stress curves of the ultrasoft transistor array and pure hydrogel). Reproduced with permission from (Li et al., 2023). Copyright 2023, Springer Nature. (g) Molecular structure of a monomer mixture, which includes a liquid crystal monomer (RM82), chain extender molecule (n-butylamine, nBA), and photoinitiator (I-369) (top left), programmable filling of the monomer mixture for substrate formation (top right), and schematic illustration of an implantable electronic device based on liquid crystal elastomers (LCEs) both as substrate and encapsulation (bottom). Reproduced with permission from (Maeng et al., 2020). Copyright 2020, Royal Society of Chemistry. (h) Depiction of a core-shell structure of Ag–Au nanocomposites, decorated with hexylamine ligands and SBS elastomer (top left), the microstructured Ag–Au nanocomposite's stretchability before and after stretching (top right), and optical image of the Ag–Au nanocomposite being stretched to 840 % (bottom). Reproduced with permission from (Choi et al., 2018). Copyright 2018, Springer Nature. (i) Molecular structure of poly(L-lactide-co-ε-caprolactone) (PLCL) elastomer and schematic illustration of structural formation of the PLCL under tensile stretching (left), and a PLCL/PP nanocomposite-based conductive probe for capturing electrophysiological (EP) signals (right). Reproduced with permission from (Han et al., 2023b). Copyright 2023, Springer Nature.

In this aspect, Fig. 1h illustrates Au-coated silver (Ag) nanowires (NWs) that were highly conductive (max. 72,600 S cm^{-1}), stretchable (max. 840%), and biocompatible (Choi et al., 2018). Electrical conduction with poly(styrene-btadiene-styrene) (SBS)-rich regions remained intact under stretching of the Ag–Au NWs due to formation of elastic micro-structured struts, which the stretchability was further improved by heat rolling-press. Using this nanocomposite, wearable and implantable soft bioelectronic devices were fabricated and integrated with human skin and swine heart for continuous electrophysiological recording as well as electrical and thermal stimulation. Fig. 1i (left) introduced an ultra-stretchable (~1600%) and biodegradable poly(l-lactide--co-ε-caprolactone) (PLCL) for the employment of different functions: (i) substrates and encapsulants in ultrathin geometries for degradable electronics, (ii) 3D free-form frameworks for soft robotics, and (iii) elaborate design layouts for soft, suture-free medical implants (Han et al., 2023b). Furthermore, two conductive elastomeric composites were prepared by blending PEDOT:PSS and molybdenum (Mo) in PLCL; these conductive composites have been demonstrated to monitor epicardial ECG and myocardial strain, and to provide electrical stimulation. The mechanical and electrical properties of various electrode materials, and advantages and disadvantages are summarized in Table 1 and Table 2, respectively.

Table 2
Advantages and disadvantages of the different electrode materials.

Classification of electrode material	Advantages	Disadvantages
Liquid metal electrode	High stretchable.	Requires high temperatures to liquify electrodes.
	Mechanical softness, outstanding electrical conductance.	Suffers from chemical corrosion under physiological conditions.
	Cheap and simple preparation.	Poor stability.
	Easy to scale up.	Complicated manufacturing process.
	Low cost, and long cycle life.	
Hydrogels	Excellent flexibility and versatility.	Conventional conductive hydrogels usually lack self-healing properties, which might be unfavorable for their application.
	Stability in physiological environments.	Complex manufacturing process.
	Outstanding biocompatibility and fully organic characteristics.	Weakened mechanical properties, flexibility and electrical conductivity.
Nanocomposite (hydrogel or elastomeric)	High electrical conductivity.	Low stability in air.
	High softness and good stretchability.	Poor interfacial property.
	Good electrochemical properties.	Incompatible with high density integration.
	Mechanically compatible.	Fabrication process not completable with etching for precise patterning.
	Electronically stable interface to interact with stable tissues.	

3. Mechanics and designs

Material advancements have notably enhanced the performance of implantable devices for dynamic organs. Yet, the role of mechanical design in these improvements is equally vital. Novel mechanical designs help address limitations due to material properties. For devices implanted in organs like the heart and bladder, balancing high electrical performance with a stable interface on moving three-dimensional shapes is essential. Despite the development of stretchable electronic materials, their modulus is still much higher than organ surfaces, affecting device conformability and biosignal quality (Sunwoo et al., 2021). Additionally, in terms of the immunological aspect, bio-implants with high modulus can negatively affect the foreign-body response, which hinders the stable operation of the device within the body over a long period (Atcha et al., 2021; Jansen et al., 2018). Therefore, efforts continue in the development of soft, implantable electronics with appropriate mechanical design strategies that transcend the inherent properties of the materials.

The quality of sensitive and weak biosignals measured on the surface of an organ is greatly influenced by the relative movement between the surface of the organ and the sensor. Thus, to ensure high-quality signals, it is crucial to minimize relative movement, particularly from the surface of the sensor consisting of the implantable electronics, by achieving conformal contact with the surface of the organ. The two surfaces can maintain this contact when $\gamma > I/2R^2$, where γ is the adhesion energy between the two layers, I is the flexural rigidity, and R is the radius of curvature, respectively. Thus, reducing flexural rigidity is an effective approach to achieve conformality on organs with a nonzero Gaussian surface. Flexural rigidity, I, is proportional to Ebh^3, where E is Young's modulus, b is the width, and h is the thickness of the layer, respectively. Therefore, flexural rigidity can be reduced either by lowering the effective modulus of the material composing the substrate or by decreasing its thickness, with the latter having a significantly greater effect.

Early research on soft, implantable electronics introduced by Kim et al. utilized a strategy of thickness adjustment. Brittle silicon-based materials and devices exhibited low flexural rigidity as the thickness decreased, allowing for conformal integration with three-dimensional structure of organ surfaces (Fig. 2a) (Viventi et al., 2010). Such electronics possessed such low flexural rigidity that they deformed under the capillary force exerted by moisture on the surface of an organ, particularly when the sensor array was brought close to the organ, they

Table 1
Mechanical and electrical properties of the different electrode materials.

Classification of electrode material	Name of material	Young's modulus	Stretchability	Conductivity	Ref
Liquid metal electrode	Free-standing Ag on SBS mat	Very much low	1500	10^5 S cm^{-1}	Zhuang et al. (2023)
	GaIn alloy	1.055 MPa	Almost infinite	4 Ω	Guo and Liu (2017)
	Cu film	NA	1000 cycles at 300% strain	3.8×10^4 S cm^{-1}	(S. Wang et al., 2022)
Hydrogels	CNTs	10 kPa	NA	~70 S cm^{-1}	Sekitani et al. (2016)
	Gelatin-based conductive film	20–420 kPa (NA)	NA	10.48 mS cm^{-1}	Chen et al. (2024)
	Bi-continuous conducting polymer	<1 MPa	>400%	>11 S cm^{-1}	Zhou et al. (2023)
	PEDOT:PSS	650 kPa	1000 cycles at a strain of 30%	9 S m^{-1}	Wang et al. (2023)
Nanocomposite (hydrogel or elastomeric)	Ag–Au core-sheath	~20 MPa	266%	41850 S cm^{-1}	Choi et al. (2018)
	PLCL/PEDOT:PSS	NA	550%	220 S cm^{-1}	Han et al. (2023b)
	PVA/PA/NH2-POSS	361 kPa	363%	2.41 S m^{-1}	Shao et al. (2020)
	CNTs-GF	10 kPa	NA	1 mS m^{-1}	Tringides et al. (2021)
	MWCNT/SEBS	5.1 MPa	400%	1.1 S cm^{-1}	(S. Wang et al., 2022)

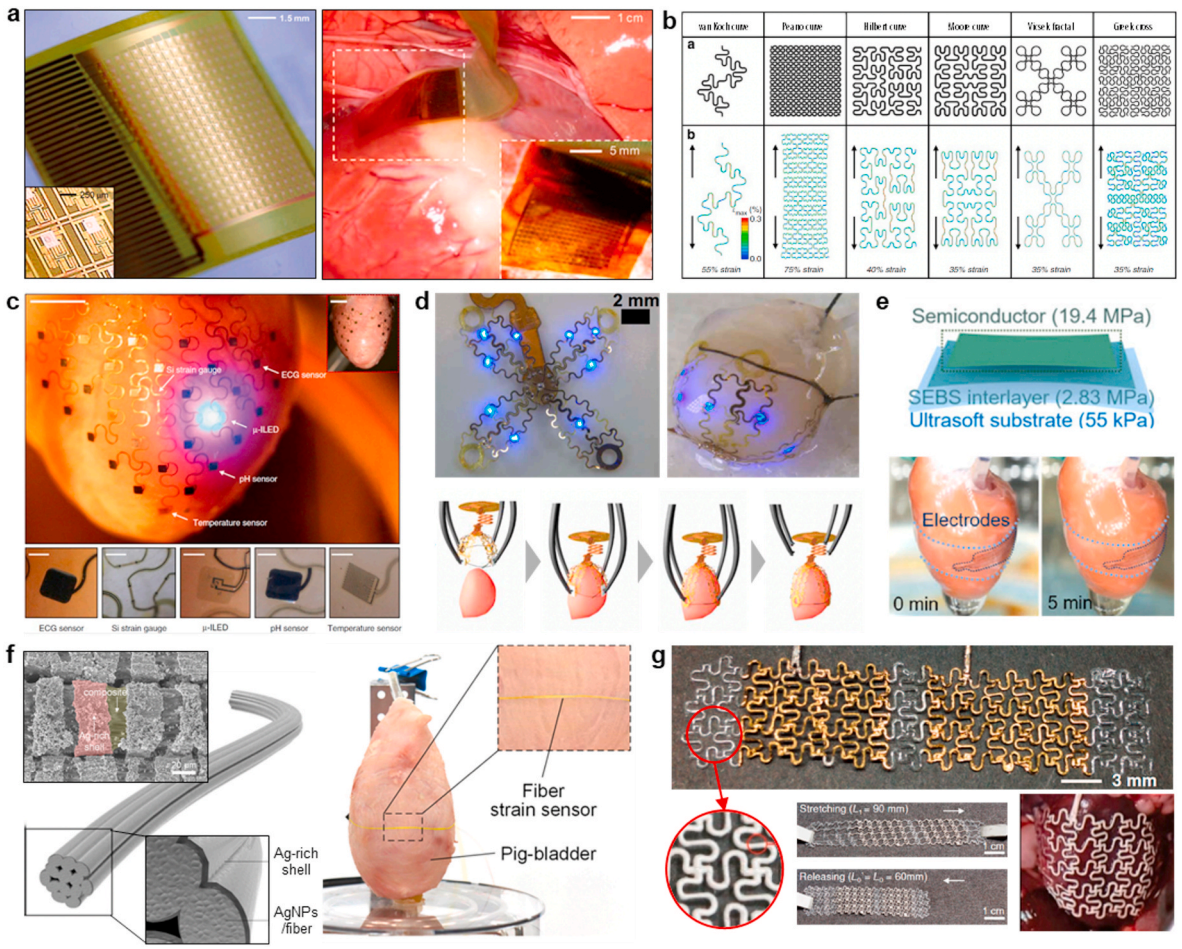

Fig. 2. Methodology on mechanical designs to achieve conformal contact of implantable electronics to dynamic organs. (a) Flexible, high-density electrode array for mapping cardiac electrophysiology, which was fabricated by adjusting thickness of the entire system to improve conformal attachment (left), and photograph of the flexible electronic system coupling to the cardiac tissues induced by surface tension (right). Reproduced with permission from (Viventi et al., 2010). Copyright 2010, AAAS. (b) Various types of theoretical fractal structures that can reduce the flexural rigidity of electronic components including electrodes, or substrate. Reproduced with permission (Fan et al., 2014). Copyright 2014, Springer Nature. (c) Thin, flexible electronic heart socks formed with diverse sensors connected by serpentine, S-shaped interconnects (top), and images of the configuration of each sensor such as ECG, strain, μ-LED, pH, and temperature sensors, respectively (bottom). Reproduced with permission from (Xu et al., 2014). Copyright 2014, Springer Nature. (d) Non-soft materials-based electronic system engineered with layout and geometry, enabled to conformally wrap around a dynamic organ (top), and sequential illustration of applying the device to a heart model (bottom). Reproduced with permission from (Ausra et al., 2022). Copyright 2022, AAAS. (e) Description of employing an interlayer with an appropriate modulus to minimize the mechanical mismatch between the layer attached to the organ and electronic component. (top), and image of the device seamlessly applied to the heart (bottom). Reproduced with permission from (Li et al., 2023). Copyright 2023, Springer Nature. (f) Schematic of a 1D stretchable electronic sensor consisting of AgNPs fiber coated with an Ag-rich shell, with scanning electron microscopy (SEM) images of the fiber in the inset (left), and photograph of a fiber-shaped stretchable strain sensor integrated with a pig model for monitoring volume changes of the bladder (right). Reproduced with permission from (J. Lee et al., 2018). Copyright 2018, American Chemical Society. (g) Photograph of a serpentine-bodied epicardial mesh (top), uniaxial tension test of the elastic epicardial mesh after 50% stretching (bottom left), and photograph of the epicardial mesh implanted in the heart (bottom right). Reproduced with permission from (Park et al., 2016). Copyright 2016, AAAS.

adhered and conformed to the surface. Another approach was to utilize or modify various structural shapes or geometries. Fan et al. significantly decreased flexural rigidity by structural modifications to thin films of electronic materials or devices into deterministic fractal motifs, as illustrated in Fig. 2b (Fan et al., 2014). Compared to existing sheet types, structures engineered with fractal motifs can effectively reduce bending stiffness. The curved, repetitive structure provides additional space which provides a lower effective Young's modulus and makes the unit cells of a fractal structure can stretch, bend, and rotate more easily compared to a typical planner structure. Thus, during stretching and bending, providing sufficient elasticity to form a seamless interface for a variety of three-dimensional configurations. Xu et al. developed an organ-specific electronic system using a 3D-printed heart model, as shown in Fig. 2c (Xu et al., 2014). They placed multiple sensors on an elastomer layer in an island configuration, connecting each sensor with stretchable s-shaped interconnects. This assembly was transferred onto the 3D-printed heart model and encapsulated with a soft layer that precisely matched to the heart's shape. The overall design minimized strains of the devices on the island, and distributed the stress to the stretchable interconnects, allowing for conformal contacts to organs with complex shapes while providing robust sensing capabilities. However, designs that can cover the entire tissue rather than specific regions not only has the ability to apply to a broad range of tissues, but also provides accurate diagnosis and detailed information through monitoring of the overall tissue.

Implantable electronics engineered to completely cover three-dimensional contours of an organ for either monitoring or stimulation involves cardiac stimulation and recording device introduced by Ausra et al. The overall system was designed with a four-petaled mesh array in a serpentine pattern to allow effective stretching and minimize plastic deformation, as shown in Fig. 2d (Ausra et al., 2022). However, the device's inability to naturally attach to the surface of the heart

necessitated the use of sutures for securing, presenting limitations in deployment and operation.

Large differences in mechanical modulus between electronic materials and tissues often leads to material cracks due to organ deformation. Li et al. tackled this issue with a hybrid structure, inserting a moderate-modulus layer between the soft tissue and the stiff semiconductor layer, as illustrated in Fig. 2e (Li et al., 2023). This interlayer effectively absorbs strain from organ movements, preventing cracks and ensuring stable contact with the organ's dynamic contours. Additionally, if the system surface in contact with the tissue is similar to or not significantly different from the tissue's modulus, stress and strain at the interface can be minimized, which eventually enabled to suppress inflammation and fibrosis and minimizes immunological issues during prolonged use. On the other hand, Lee et al. exploited cracks to enhance implantable electronics, developing a one-dimensional fiber sensor embedded with Ag nanoparticles (J. Lee et al., 2018). As shown in Fig. 2f, highly stretchable and sensitive sensors measured strains through resistance changes caused by cracks in the Ag-rich layer. Unlike conventional approaches that eliminate the issue of mechanical mismatch, this technique leveraged them for design. The one-dimensional fiber offers better conformality on three-dimensional shapes than two-dimensional alternatives. By wrapping around a porcine bladder, they achieved stable measurement of expansion in one direction, with the potential for multi-directional development. By weaving the fibers into flexible textiles, it could be possible to utilize them as new types of sensors that are suitable for complex, nonplanar substrates.

Park et al. demonstrated a system that can directly provide electrical stimulation to the heart of a mouse using an epicardial mesh made up of an elastic material with electrical conductivity (Park et al., 2016). As shown in Fig. 2g, an epicardium-like substrate was mechanically integrated into the heart, acting like a structural element of the cardiac chamber. The system includes nanocomposites of ligand-exchanged silver nanowires (LE-AgNW) and SBS rubber, which exhibits high conductivity, superior elasticity, and efficient shape recovery capabilities. In particular, nanocomposites with a low modulus of ~0.5 MPa were processed into mesh shapes, resulting in meshes with moduli in the range of 3–40 KPa. Considering that epicardial tissue with a thickness of 2 mm has ~35 KPa, the interface between the implantable system and the cardiac tissue could be seamlessly integrated without hindering the volumetric expansion. The advancement in the mechanical processing of high-performance, biocompatible conductive soft materials paves the way for the development of implantable electronics capable of fully encircling a dynamic organ. Such strategies allow comprehensive three-dimensional monitoring and targeted stimulation while exerting minimal influence on the functionality of organs.

4. Soft, implantable bladder-integrated electronics

Soft implantable electronics can be seamlessly integrated with the curved, time-dynamic surfaces of internal organs, facilitating the acquisition of high-fidelity physiological signals and delivery of efficient feedback stimulation. Among various internal organs, urinary bladder exhibits unique characteristics that experiences significant volume changes (~300 %) during the storage and urination phases, which would be quite challenging for the application of soft implantable electronics (De Groat, 2006; Yoshimura and De Groat, 1997). For bladder disorders, e.g., overactive bladder (OAB) and underactive bladder (UAB), have been proposed various strategies such as device fixation using sutures on the bladder, designs with high adhesion properties, and enveloping configurations (Jang et al., 2020; Mickle et al., 2019; B. Oh et al., 2023; Stauffer et al., 2018). Since clinical interventions and drugs have often been ineffective or associated with significant side effects in patients with severe symptoms (Harada et al., 2010; Riedl et al., 2000; van Kerrebroeck et al., 2007), there has been the need for long-term stable signal measurements and treatment options facilitated by soft implantable electronics. Fixation strategies, monitoring/stimulation functionalities and relevant diseases for the bladder are summarized in Table 3.

Given the dynamic mechanical nature of the bladder, strain gauges have been utilized as a common tool to monitor functionalities of the bladder. Fig. 3a represents a patch-type capacitive strain gauge for bladder monitoring (Stauffer et al., 2018). The proposed system exploited biocompatible and highly conductive Au-titanium dioxide (TiO_2) nanowires as the sensing element, integrated with a soft silicone elastomer to form a planar plate-type capacitor. Variations in strain led to changes in capacitance, affecting the resonance frequency of a connected electromagnetic coil. The frequency shift was wirelessly detected in a real-time mode by a portable readout system. Efficacy of such system was demonstrated *ex vivo* in a porcine bladder by simulating water filling and releasing cycles, and the system successfully estimated voided volume of water. Mechanical motion of the bladder is controlled by electrical signals originating from the nerves; thus electromyography (EMG) signal can serve as additional information to assess the bladder's condition (Jang et al., 2020; Lee et al., 2023; B. Oh et al., 2023). Fig. 3b presents a multifunctional bladder activity sensor based on PAAm hydrogel for continuous monitoring of OAB. The hydrogel substrate exhibits ultra-soft characteristics with a low modulus of 1 kPa, resulting in minimal mechanical impact on the urinary bladder (B. Oh et al., 2023). Additionally, the incorporation of an anti-swelling layer and a hydrogel-based adhesive layer allowed for stable fixation and operation onto the urinary bladder. Measured peaks in the resistance of strain gauge indicated maximum contraction of the bladder, while the root mean square (RMS) of the EMG signal determined the time at which EMG activation had increased. Multi-modal measurements allowed for precise determination of the urination point and voiding parameters, demonstrating the potential to provide differences in normal and OAB models. Beyond the monitoring options, desired modulation of bladder function can be a powerful tool to alleviate or eliminate clinical symptoms. Fig. 3c demonstrates a fully implantable, wireless closed-loop system with optoelectronic stimulation (a pair of micro-light-emitting-diodes (μ-LEDs)) and sensing (strain gauge; carbon black/silicone elastomer composite) module (Mickle et al., 2019). The device completely enveloped the bladder by connecting buckles at both ends and maintained robust attachment to the bladder via sutures for a long-term operation. The bladder was optogenetically controlled using viral vectors, which successfully increased voiding intervals upon exposure to green light to alleviate symptoms of OAB. A closed-loop software deployed on a handheld device enabled real-time visualization of operational data and automated control interface through detection of the abnormal urination cycles. UAB or detrusor underactivity (DUA) is another prevalent symptom characterized by the inability to naturally release urine. If left untreated, it can lead to serious complications such as urinary retention and chronic kidney failure (Drake et al., 2014; Hoag and Gani, 2015). Fig. 3d illustrates an expandable electronic complex equipped with multi-modal monitoring components and optoelectronic modulation for UAB (Jang et al., 2020). The interlocked system architecture of electronic web (E-web) and thread (E-thread) facilitated scalable design layout and stable performance of the overall electronic system, which maintained intimate contacts over the entire surface of the elastic urinary bladder without the need for sutures. A total of seven electronic devices were integrated into a thin, strip-type E-thread for high-quality, accurate information and efficient optoelectronic excitation of the entire bladder area. Guided by a custom flowchart, bladder sensors sequentially detected and analyzed bladder status, and allowed for urine release at the desired time. In addition to optoelectronic stimulation, other stimulation tools have been studied for bladder contraction. Fig. 3e illustrates ultra-compliant implantable electronic devices capable of inducing bladder contraction through direct electrical stimulation (Yan et al., 2019). Bladder is entirely surrounded by the detrusor muscle, which induces induce voiding through contraction via electrical stimulation. A carbon nanotube silicone/elastomer composite was utilized as the strain gauge, while a platinum

Table 3
Monitoring/stimulation functionalities, fixation strategies and relevant diseases for the urinary bladder.

Monitoring technologies (Materials)	Stimulation technologies (Materials)	fixation strategies (Substrate materials)	Relevant diseases	Ref.
Capacitive strain gauge (Au–TiO_2 nanowire)	– –	sutures	OAB/UAB	Stauffer et al. (2018)
Resistive strain gauge (Au)	– –	Hydrogel adhesive	OAB/UAB	Hannah et al. (2019)
Resistive strain gauge (EGain), EMG electrodes (Platinum black)	– –	Hydrogel adhesive (PAAm hydrogel)	OAB/UAB	(B. Oh et al., 2023)
Resistive strain gauge (Carbon black/ Ecoflex composite)	Optical (μ-LED)	Enveloping with sutures	OAB	Mickle et al. (2019)
Resistive strain gauge (Si nanomembrane), Resistive temperature meter (Pt), EMG electrodes (Au)	Optical (μ-LED)	Enveloping without sutures	UAB	Jang et al. (2020)
Resistive strain gauge (CNT)	Electrical (Pt/PDMS composite)	sutures	UAB	Yan et al. (2019)
Resistive strain gauge (Si nanomembrane), EMG electrodes (Au)	Electrical (Platinum black)	Enveloping without sutures	UAB	Lee et al. (2023)
	Physical (Thermo-responsive PNIPAAM hydrogel)	Enveloping without sutures	UAB	Yang et al. (2018)
Capacitive strain gauge (Wrinkled Au)	Physical (Shape memory alloy-based actuator)	-(Polyurethane)	UAB	Arab Hassani et al. (2020)
–	Magnetic field-induced physical (NdFeB microparticles)	Enveloping without sutures (Ecoflex, PAAm hydrogel)	UAB	(Y. Yang et al., 2022)

nanoparticles/silicone elastomer composite served as the stimulation electrode. These soft electronics overcame drawbacks associated with traditional rigid electronics, such as electrode detachment and lead breakage, and enable stable electrical stimulation using multiple electrodes. *In vivo* operation of the system validated that bladder contraction through electrical stimulation achieved voiding efficiency similar to normal urination. Physical bladder compression techniques can offer advantages by minimizing influence on neighboring muscles or nerves during urination induction. Compression technique options include thermo-responsive hydrogel and shape memory alloy (SMA) actuator, and magnetic soft robots (Arab Hassani et al., 2020; Yang et al., 2018; Y. Yang et al., 2022). Fig. 3f shows an example system for physical bladder control, incorporating soft sensors and flexible SMA-based actuators (Arab Hassani et al., 2020). Wrinkled interdigitated electrodes on the acrylic elastomer layer served as capacitive strain gauge for bladder volume measurement. Additionally, SMA springs assisted in maintaining contact between the sensor and bladder surface, ensuring precise volume detection. By applying voltage to the SMA components, the actuator effectively modulated bladder function, resulting in high voiding efficiency observed in the rat bladder *in vivo*.

5. Soft, implantable electronics for heart

Cardiovascular diseases (CVDs), including coronary artery diseases, stroke, high blood pressure, and heart failure, stand as the leading cause of death globally, responsible for 18.5 million deaths, approximately one-third of all mortality (Roth et al., 2020; Townsend et al., 2022). Consequently, the development of effective cardiac diagnostic/therapeutic technologies is paramount to ensure overall health and well-being. However, conventional bulky and rigid cardiac devices posed significant drawbacks in terms of comfort, long-term viability, and accurate data collection. In this respect, the evolution toward pliable, implantable electronics that seamlessly integrate with soft and time-dynamic heart is imperative for revolutionizing cardiac healthcare, ultimately leading to improved patient outcomes and a better quality of life (Summary of soft, implantable cardiac electronics appears in Table 4).

Precise monitor of electrocardiography (ECG) signals with high spatial and temporal resolutions is a fundamental yet effective method for elucidating cardiac electrophysiology and functions. In this regard, multielectrode arrays (MEAs) have been developed in thin, flexible configurations that can be conformally integrated into the dynamic, curved surface of the heart, enabling real-time multiplexed measurement of ECGs (Viventi et al., 2010), even with additional electrical functions such as strain/pH/temperature sensing and optical/thermal actuation (Xu et al., 2014). For example, Fig. 4a illustrates active 4x4 MEA with stretchability and nonthrombogenicity for long-term mapping of ECG signals (Wonryung Lee et al., 2018). The electronics, primarily comprised of organic electrochemical transistors (OECTs) with PEDOT:PSS as an active layer and Au as electrodes, were fabricated within a parylene-based honeycomb grid substrate and encapsulant, with a total thickness of 2.6 μm. Such ultrathin device exhibited high flexibility and stretchability and could conformally contact the surface of a rat heart, minimizing motion artifact-induced noise. Moreover, OECTs exhibited a transconductance 100 times higher than that of silicon field-effect-transistor (Si FET), and the use of poly (3-methoxypropyl acrylate) (PMC3A) as the outermost layer suppressed the formation of blood clots between the device and heart surface, allowing for *in vivo* recording with a high signal-to-noise ratio (52 dB). In addition to such diagnostic function, stimulation capability holds significant potential for the therapy of CVDs. Fig. 4b demonstrates a wireless, flexible, implantable electronics capable of both electrical and optical stimulation (Gutruf et al., 2019). The system comprised two platinum (Pt) electrodes and a μ-LED, connected to the receiver and control units via serpentine interconnects. These components were attached to the right ventricle of an isolated heart within a temperature-controlled Langendorff system, delivering electrical and optical pulses to the heart. These stimulations generated and propagated action potentials, demonstrating the pacing capability to regulate heart rate to preset frequencies (>400 BPM) higher than the intrinsic heart rate (~300 BPM). Here, optogenetic pacing utilized light-activated proteins (channelrhodopsin 2 (ChR2))-expressing hearts to induce depolarization and action potentials in response to optical stimulus. A similar system, but in a 3D-configurable design, has extended the potential of optogenetic pacing, combining it with electrical recording and on-device computation, for closed-loop management of cardiac diseases in freely moving small animals (Ausra et al., 2022).

Devices based on soft and stretchable polymers can mitigate mechanical mismatches with cardiac tissue, ensuring reliable functionality in response to the rhythmic contractions of the heart. Fig. 4c displays an inorganic-organic hybrid composite-based stretchable, implantable cardiac mesh (Choi et al., 2018). Elastic polymer, SBS, was utilized as substrate/encapsulation, while an Ag core-Au sheath nanowires/SBS composite, engineered to possess biocompatibility, high conductivity (41,850 S cm^{-1}), and stretchability (~266%) in the presence of an appropriate surfactant, served as multichannel sensing electrodes. Due

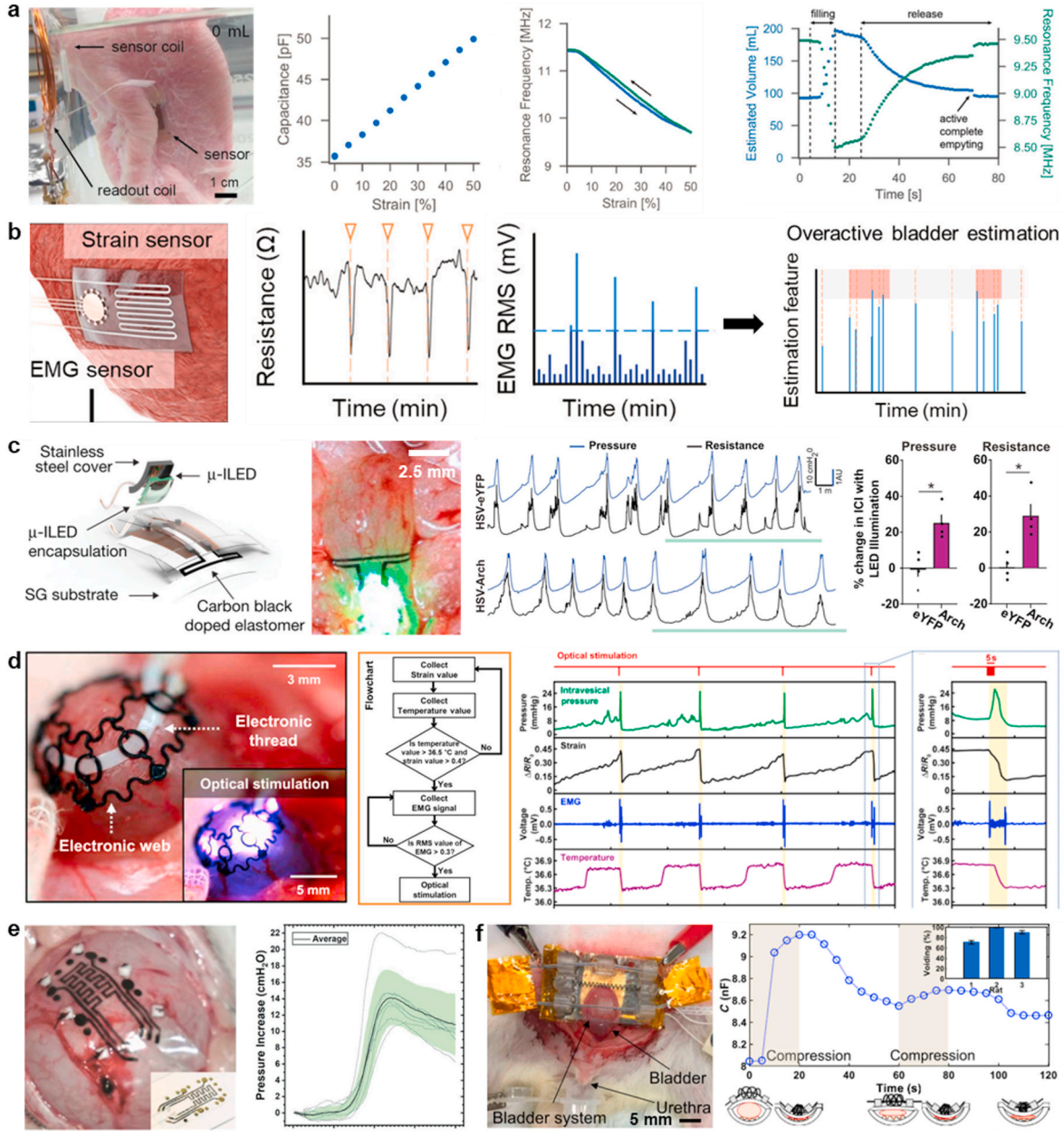

Fig. 3. Soft, implantable bladder-integrated electronics. (a) Optical image showing a stretchable Au–TiO_2 nanowire sensor sutured onto a fresh *ex vivo* pig bladder and a wireless readout coil (left), capacitance change of the sensor and subsequent resonance frequency shift in response to mechanical strains (middle), and continuous monitoring results during the bladder's water filling and releasing phases (right). Reproduced with permission from (Stauffer et al., 2018). Copyright 2018, Wiley-VCH GmbH. (b) Schematic illustration of a stretchable and tissue-adhesive multifunctional sensor for monitoring bladder activity (left), strain and root-mean-square (RMS) of the electromyography (EMG) signal for the analysis of the voiding events (middle), and estimated overactive bladder (OAB) diagnosis based on the analysis results (right). Reproduced with permission from (Hannah et al., 2019). Copyright 2023, Springer Nature. (c) Exploded view of an implantable electronic system incorporated with a strain gauge based on carbon black (CB)-silicone composite and an optoelectronic device, and an image of the electronic system wrapped around the rat bladder in the inset (left), and representative traces and grouped data of electrical resistance (strain gauge) and intravesical pressure (commercial pressure sensor) in HSV-Arch-injected animals compared to HSV-eYFP-injected controls, with and without green light illumination (right). Reproduced with permission from (Mickle et al., 2019). Copyright 2019, Wiley-VCH GmbH. (d) Photograph of a soft electronic complex, configured with electronic web for elastomeric framework and electronic thread for comprehensive functional activities, integrated into the urinary bladder, with an optical stimulation image in the inset (left), customized protocol for analyzing biological parameters and manipulating optical stimulation in a real-time mode (middle), and comprehensive dataset of the measured parameters from the electronic complex (strain, EMG, and temperature) and commercial pressure sensor (intravesical pressure) in the detrusor underactivity (DUA) mouse model (right). Reproduced with permission from (Jang et al., 2020). Copyright 2020, AAAS. (e) Ultra-compliant device sutured onto the feline bladder wall for monitoring and direct electrical stimulation, with a device image in the inset (left), and stimulation-induced intravesical pressure changes for bladder contractions (right). Reproduced with permission from (Yan et al., 2019). Copyright 2019, Wiley-VCH GmbH. (f) Bladder-integrated system comprising a capacitive sensor and shape memory alloy (SMA) based actuator with high voiding efficiency (left), and recorded capacitance characteristics of the system during mechanical compression, with voiding efficiency results for three rats depicted in the inset (right) Reproduced with permission from (Arab Hassani et al., 2020). Copyright 2020, AAAS.

Table 4
Summary of soft, implantable, cardiac electronics.

Structure	Materials	Functions	Features	Ref
Membrane	Si	ECG mapping	2016 transistors	Viventi et al. (2010)
Membrane	Au	Optical mapping, ECG, Pacing, Strain, pH, Temp., Heater	3D model	Xu et al. (2014)
Mesh	PMC3A, PEDOT:PSS, Au	ECG mapping	4x4 organic electrochemical transistors	(Wonryung Lee et al., 2018)
Mesh	AgNW on SBS	ECG, Pacing	Highly-stretchable	Park et al. (2016)
Mesh	Ag–Au NW on SBS	ECG, Pacing	Highly-stretchable	Choi et al. (2018)
Mesh	Ag–Au wire, Pt black, SBS	ECG, Pacing	Highly-stretchable	Sunwoo et al. (2020)
Mesh	P3HT, AgNP + AgNW on PDMS	ECG, Pacing, Strain, Temp., Heater	Stretchable, 5x5 organic field-effect-transistors	Sim et al. (2020)
Mesh	Cu/Pt	Pacing, ECG	Wireless, Optogenetic stimulation, Closed-loop	Ausra et al. (2022)
Mesh	PEDOT:PSS on PLCL	ECG, Pacing, Strain	Stretchable, Biodegradable, Suture-free	Han et al. (2023b)
Patch	Cu	Pacing	Wireless, Optogenetic stimulation	Gutruf et al. (2019)
Patch	W/Mg on PLGA	ECG, Pacing	Wireless, fully-bioresorbable, human model	Choi et al. (2021)
Patch	Mo on DCPU	ECG, Pacing	Wireless, fully-bioresorbable, human model, Closed-loop	Choi et al. (2022)
Patch	Au/ graphene-hydrogel	ECG	Bioadhesive	Deng et al. (2021)

to the soft and elastic nature, this mesh electronics could be wrapped conformally around a swine heart, reliably recording 34-channel epicardial ECG signals. Furthermore, multichannel mesh electrodes enabled myocardial voltage mapping, allowing the device to visualize clearly differentiated voltage patterns to detect acute ischemia induced by occlusion of the left anterior descending coronary artery (LAD). The mechanical compliance of polymer composite-based cardiac meshes and reliable recording/stimulation capabilities can be further found in various research studies (Park et al., 2016; Sim et al., 2020). Fig. 4d presents soft, biodegradable cardiac electronics (Han et al., 2023b), primarily comprised PLCL as substrate/encapsulation, with PLCL/PEDOT:PSS and PLCL/Mo flake composites serving for ECG recording/electrical stimulation and strain sensing, respectively. All constituent materials were biocompatible and dissolvable/disintegrable in aqueous solutions or biofluids (Han et al., 2020, 2023a), providing an opportunity to eliminate the risk of device retrieval after operation for a desired period. Furthermore, stingray barb-inspired straps along with tailored open-mesh body structure, facilitated suture-free device integration into a rat heart by delicately fastening/releasing the straps, akin to wearing a halter-neck dress. For 8 weeks of implantation, the cardiac jacket maintained not only structural integrity, thanks to the fit/robust integration and hydrophobic nature of PLCL with a high molecular weight (Mn, ~140k), but also electrical functions (ECG recording and pacing) without substantial degradation, owing to the softness/-stretchability of the electronic components. These results promised the potential for long-term treatment of cardiac diseases in clinically relevant periods, while minimizing burdens on patients. Fig. 4e illustrates a wireless, battery-free, fully-bioresorbable pacemaker composed of biodegradable metals (tungsten (W)/magnesium (Mg))-based inductive coils and electrodes, Si nanomembrane-based diode, and poly (lactic-co-glycolic acid) (PLGA) substrate/encapsulation (Choi et al., 2021). Surgically affixed to the surfaces of hearts in mouse, rat, rabbit, canine, and human models, the pacemaker received power through resonant inductive coupling between an external transmission antenna to the receiving coil of the device, delivering electrical stimulation for postoperative control of cardiac rate and rhythm. After a defined operational timescale, the device completely dissolved and resorbed by natural biological processes, with no adverse effects observed in organs and overall health conditions. Recently, a combined utilization of the bioresorbable cardiac device with a time-synchronized, wireless network of skin-interfaced modules, including hemodynamic, respiratory, and cardiac sensors, as well as haptic actuator, demonstrated the feasibility of autonomous electrotherapy tailored to match postoperative needs (Fig. 4f) (Choi et al., 2022). This closed-loop network wirelessly tracked cardiopulmonary health and physical activity in real time, provided multi-haptic feedback for patient awareness, and autonomously regulated cardiac rhythms using algorithms without the need for physician intervention. Relevant tests conducted with rat, canine, and human hearts confirmed the autonomous, rate-adaptive cardiac pacing capabilities. In clinical scenarios, the pacemaker can undergo complete dissolution after patient recovery, minimizing the risk of a second surgery while the skin-integrated modules can be retrieved, suggesting practical potential for temporary postoperative diagnosis and therapy.

6. Summary and conclusions

Soft, implantable electronics described here introduce a comprehensive range of concepts, various types of materials, mechanical designs, and applications tailored for dynamic organs. Coupled with advancements in soft, mechanically compliant electronic materials, novel mechanical design strategies enabled implantable devices to achieve conformal contacts with the curvilinear surfaces of organs, mitigated mechanical mismatch with biological tissues, and minimized motion artifacts, thereby ensuring reliable functionality within the human body. These innovations extend to time-dynamic and deformable organs such as bladder and heart, offering diagnostic and therapeutic interventions with diverse modalities.

7. Future perspectives

Despite the remarkable strides, further advancements are needed in materials and mechanical aspects to evolve current soft, implantable electronics towards practical and clinically relevant tools. For chronic implantation, it is essential to address foreign body reactions, which are particularly important for diseases – underactive bladder and bradycardia – that do not have available treatment options. Such inflammatory and fibrotic reactions lead to the formation of a dense, electrically inactive fibrous capsule around implants, potentially disrupting the device-tissue interface and imposing substantial physical stress on dynamic organ movements. To tackle this challenge, comprehensive and long-term evaluations of biocompatibility and surface treatments to regulate anti-fibrosis and cell adhesion can be considered. Also, a minimally invasive implantation approach provides a promising way in mitigating such reactions, as well as potential inflammation and infection. This strategy can be realized through syringe-injectable devices, bioadhesive materials, and 3D-configurable, suture-free device designs. Incorporation of unique material properties can enhance device functionality. Bioresorbable materials-based implantable devices offer a solution to safety concerns by eliminating the need for secondary surgeries, since these devices degrade or dissolve harmlessly within the body after operation for designed timescales. In terms of device stability,

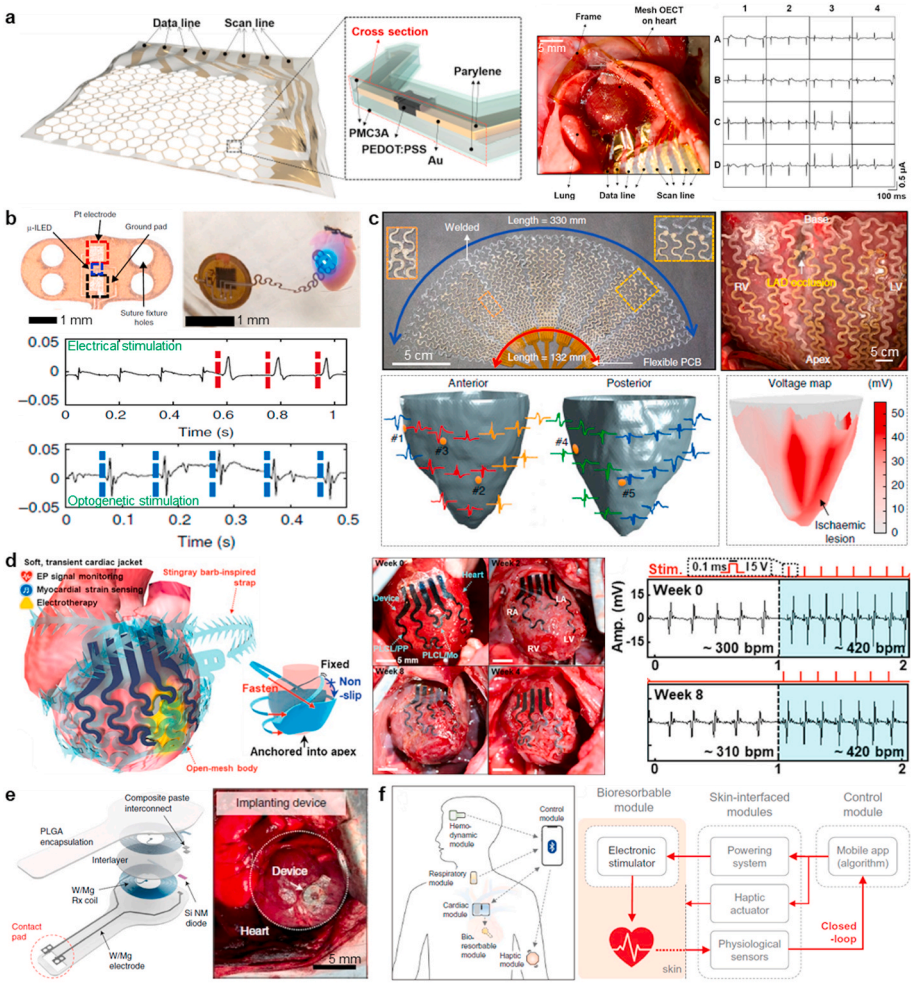

Fig. 4. Soft, implantable cardiac electronics. (a) Illustration of a stretchable, organic electrochemical transistor (OECT) array designed for cardiac monitoring, with a magnified device structure in the inset (left), and recording of electrocardiography (ECG) signals by a multiplexed 4x4 OECT array on the heart of a rat (right). Reproduced with permission from (Wonryung Lee et al., 2018). Copyright 2018, AAAS. (b) Optical images of a wireless, battery-free, implantable stimulator featuring optogenetic and electrical pacing capabilities and the device sutured onto a rat heart (top), and ECG signals recorded under both *in vivo* electrical (middle; 5 ms, ~7 Hz) and *ex vivo* optogenetic (bottom; 250 ms, 10 Hz) stimulations. Reproduced with permission from (Gutruf et al., 2019). Copyright 2019, Springer Nature. (c) Images of a silver (Ag) core-gold (Au) sheath nanocomposite-based stretchable, multifunctional mesh-type electronics for monitoring and stimulation of cardiac functions (top left) and the device implanted onto a swine heart *in vivo*, where RV, LV, and LAD refer to right and left ventricles and left anterior descending coronary artery, respectively (top right), 3D reconstructed images of the heart with measured epicardial ECG signals (bottom left), and voltage map constructed by interpolating local epicardial electrograms of acute ischemia-induced heart using the scattered-interpolant class and the natural neighbor interpolation algorithm (bottom right). Reproduced with permission from (Choi et al., 2018). Copyright 2018, Springer Nature. (d) Schematic illustrations of a stretchable, biodegradable, multifunctional cardiac jacket and suture-free device integration process (left), optical images of the device implanted on a rat heart after 0, 2, 4, and 8 weeks of implantation (middle), and epicardial ECG signals obtained before and after electrical stimulation (duration, 5 ms; frequency, 7 Hz) at week 0 and 8 of implantation (right). Reproduced with permission from (Han et al., 2023b). Copyright 2023, Springer Nature. (e) Exploded-view drawing of a wireless, fully-bioresorbable pacemaker (left), and photograph of the device sutured to the ventricular epicardium of an *in vivo* canine model (right). Reproduced with permission from (Choi et al., 2021). Copyright 2021, Springer Nature. (f) Schematic description (left) and operational diagram (right) of a transient closed-loop system with diverse skin-interfaced modules for autonomous and wireless cardiac therapy. Reproduced with permission from (Choi et al., 2022). Copyright 2022, AAAS.

self-healing materials, that can autonomously repair fatigue-induced cracks or mechanical failures, secure stable device operation for an extended lifetime. Adaptive designs capable of adjusting the mechanical properties according to surrounding environment, e.g., shape memory materials, can facilitate both the handling of thin and soft devices during implantation and seamless integration with target organs. Meanwhile, implementation of closed-loop systems marks a significant leap toward personalized, proactive, and precise therapy and have the potential to revolutionize the clinical translation of innovative soft, implantable electronics. To achieve this ultimate goal, simultaneous development of multi-modal devices for real-time monitoring of physiological parameters, along with robust systems for data processing, analysis, and real-time feedback control and regulatory compliances for safety and efficacy, is imperative.

CRediT authorship contribution statement

Won Bae Han: Writing – original draft, Investigation, Conceptualization. **Tae-Min Jang:** Writing – original draft, Investigation. **Beom-june Shin:** Writing – original draft, Investigation. **Venkata Ramesh Naganaboina:** Writing – original draft, Investigation. **Woon-Hong Yeo:** Writing – review & editing. **Suk-Won Hwang:** Writing – review & editing, Supervision, Conceptualization.

Declaration of competing interest

The authors declare that they have no known competing financial interests or personal relationships that could have appeared to influence the work reported in this paper.

Data availability

No data was used for the research described in the article.

Acknowledgements

This work is funded by Korea Institute of Science and Technology (KIST) Institutional Program (2E32501), the National Research Foundation of Korea (NRF) grant funded by the Korea government (the Ministry of Science, ICT, MSIT) (RS-2022-00165524), the development of technologies for electroceuticals of National Research Foundation (NRF) funded by the Korean government (MSIT) (RS-2023-00220534), and the Ministry of the Science and ICT(MSIT), under the ICT Creative Consilience program (IITP-2023-2020-0-01819) supervised by the IITP (Institute for Information & communications Technology Planning & Evaluation) and Start up Pioneering in Research and Innovation (SPRINT) through the Commercialization Promotion Agency for R&D Outcomes(COMPA) grant funded by the Korea government(Ministry of Science and ICT) (1711198921). Also, we acknowledge the support of the National Science Foundation (CCSS-2152638) and the IEN Center Grant from the Georgia Tech Institute for Electronics and Nanotechnology.

References

Arab Hassani, F., Jin, H., Yokota, T., Someya, T., Thakor, N.V., 2020. Sci. Adv. 6, 412–413.
Atcha, H., Jairaman, A., Holt, J.R., Meli, V.S., Nagalla, R.R., Veerasubramanian, P.K., Brumm, K.T., Lim, H.E., Othy, S., Cahalan, M.D., Pathak, M.M., Liu, W.F., 2021. Nat. Commun. 12, 3256.
Ausra, J., Madrid, M., Yin, R.T., Hanna, J., Arnott, S., Brennan, J.A., Peralta, R., Clausen, D., Bakall, J.A., Efimov, I.R., Gutruf, P., 2022. Sci. Adv. 8, 7469.
Bandodkar, A.J., You, J.M., Kim, N.H., Gu, Y., Kumar, R., Mohan, A.M.V., Kurniawan, J., Imani, S., Nakagawa, T., Parish, B., Parthasarathy, M., Mercier, P.P., Xu, S., Wang, J., 2017. Energy Environ. Sci. 10, 1581–1589.
Bartlett, M.D., Kazem, N., Powell-Palm, M.J., Huang, X., Sun, W., Malen, J.A., Majidi, C., 2017. Proc. Natl. Acad. Sci. U. S. A. 114, 2143–2148.
Baumgartner, M., Hartmann, F., Drack, M., Preninger, D., Wirthl, D., Gerstmayr, R., Lehner, L., Mao, G., Pruckner, R., Demchyshyn, S., Reiter, L., Strobel, M., Stockinger, T., Schiller, D., Kimeswenger, S., Greibich, F., Buchberger, G., Bradt, E., Hild, S., Bauer, S., Kaltenbrunner, M., 2020. Nat. Mater. 19, 1102–1109.
Byun, J., Lee, Y., Yoon, J., Lee, B., Oh, E., Chung, S., Lee, T., Cho, K.J., Kim, J., Hong, Y., 2018. Sci. Robot. 3, eaas9020.
Chen, Y., Zhou, Y., Hu, Z., Lu, W., Li, Z., Gao, N., Liu, N., Li, Y., He, J., Gao, Q., Xie, Z., Li, J., He, Y., 2024. Nano-Micro Lett. 16, 34.
Choi, S., Han, S.I., Jung, D., Hwang, H.J., Lim, C., Bae, S., Park, O.K., Tschabrunn, C.M., Lee, M., Bae, S.Y., Yu, J.W., Ryu, J.H., Lee, S.W., Park, K., Kang, P.M., Lee, W.B., Nezafat, R., Hyeon, T., Kim, D.H., 2018. Nat. Nanotechnol. 13, 1048–1056.
Choi, Y.S., Hsueh, Y.Y., Koo, J., Yang, Q., Avila, R., Hu, B., Xie, Z., Lee, G., Ning, Z., Liu, C., Xu, Y., Lee, Y.J., Zhao, W., Fang, J., Deng, Y., Lee, S.M., Vázquez-Guardado, A., Stepien, I., Yan, Y., Song, J.W., Haney, C., Oh, Y.S., Liu, W., Yun, H.J., Banks, A., MacEwan, M.R., Ameer, G.A., Ray, W.Z., Huang, Y., Xie, T., Franz, C.K., Li, S., Rogers, J.A., 2020. Nat. Commun. 11, 5990.
Choi, Y.S., Yin, R.T., Pfenniger, A., Koo, J., Avila, R., Benjamin Lee, K., Chen, S.W., Lee, G., Li, G., Qiao, Y., Murillo-Berlioz, A., Kiss, A., Han, S., Lee, S.M., Li, C., Xie, Z., Chen, Y.Y., Burrell, A., Geist, B., Jeong, H., Kim, J., Yoon, H.J., Banks, A., Kang, S.K., Zhang, Z.J., Haney, C.R., Sahakian, A.V., Johnson, D., Efimova, T., Huang, Y., Trachiotis, G.D., Knight, B.P., Arora, R.K., Efimov, I.R., Rogers, J.A., 2021. Nat. Biotechnol. 39, 1228–1238.
Choi, Y.S., Jeong, H., Yin, r.t., Avila, R., Pfenniger, A., Yoo, J., Lee, J.Y., Tzavelis, A., Lee, Y.J., Chen, S.W., Knight, H.S., Kim, S., Ahn, H.-Y., Wickerson, G., Vazquez-Guardado, A., Higbee-Dempsey, E., Russo, B.A., Napolitano, M.A., Holleran, T.J., Razzak, L.A., Miniovich, A.N., Lee, G., Geist, B., Kim, B., Han, S., Brennan, J.A., Aras, K., Kwak, S.S., Kim, J., Waters, E.A., Yang, X., Burrell, A., Chun, K.S., Liu, C., We, C., Rwei, A.Y., Spann, A.N., Banks, A., Johnson, D., Zhang, Z.J., Haney, C.R., Jin, S.H., Sahakian, A.V., Huang, Y., Trachiotis, G.D., Knight, B.P., Arora, R.K., Efimov, I.R., Rogers, J.A., 2022. Science 376, 1006.
Chung, H.U., Kim, B.H., Lee, J.Y., Lee, J., Xie, Z., Ibler, E.M., Lee, K.H., Banks, A., Jeong, J.Y., Kim, Jongwon, Ogle, C., Grande, D., Yu, Y., Jang, H., Assem, P., Ryu, D., Kwak, J.W., Namkoong, M., Park, J. Bin, Lee, Y., Kim, D.H., Ryu, A., Jeong, J., You, K., Ji, B., Liu, Z., Huo, Q., Feng, X., Deng, Y., Xu, Y., Jang, K.I., Kim, Jeonghyun, Zhang, Y., Ghaffari, R., Rand, C.M., Schau, M., Hamvas, A., Weese-Mayer, D.E., Huang, Y., Lee, S.M., Lee, C.H., Shanbhag, N.R., Paller, A.S., Xu, S., Rogers, J.A., 2019. Science 363, eaau0780.
De Groat, W.C., 2006. Br. J. Pharmacol. 147, S25.
Deng, J., Yuk, H., Wu, J., Varela, C.E., Chen, X., Roche, E.T., Guo, C.F., Zhao, X., 2021. Nat. Mater. 20, 229–236.
Drake, M.J., Williams, J., Bijos, D.A., 2014. Nat. Rev. Urol. 11, 454–464.
Fan, J.A., Yeo, W.H., Su, Y., Hattori, Y., Lee, W., Jung, S.Y., Zhang, Y., Liu, Z., Cheng, H., Falgout, L., Bajema, M., Coleman, T., Gregoire, D., Larsen, R.J., Huang, Y., Rogers, J. A., 2014. Nat. Commun. 5, 3266.
Guo, R., Liu, J., 2017. J. Micromech. Microeng. 27, 104002.
Gutruf, P., Yin, R.T., Lee, K.B., Ausra, J., Brennan, J.A., Qiao, Y., Xie, Z., Peralta, R., Talarico, O., Murillo, A., Chen, S.W., Leshock, J.P., Haney, C.R., Waters, E.A., Zhang, C., Luan, H., Huang, Y., Trachiotis, G., Efimov, I.R., Rogers, J.A., 2019. Nat. Commun. 10, 5742.
Han, W.B., Heo, S.Y., Kim, D., Yang, S.M., Ko, G.J., Lee, G.J., Kim, D.J., Rajaram, K., Lee, J.H., Shin, J.W., Jang, T.M., Han, S., Kang, H., Lim, J.H., Kim, D.H., Kim, S.H., Song, Y.M., Hwang, S.W., 2023a. Sci. Adv. 9, eadf5883.
Han, W.B., Ko, G.J., Lee, K.G., Kim, D., Lee, J.H., Yang, S.M., Kim, D.J., Shin, J.W., Jang, T.M., Han, S., Zhou, H., Kang, H., Lim, J.H., Rajaram, K., Cheng, H., Park, Y.D., Kim, S.H., Hwang, S.W., 2023b. Nat. Commun. 14, 2263.
Han, W.B., Lee, J.H., Shin, J.W., Hwang, S.W., 2020. Adv. Mater. 32, 2002211.
Han, W.B., Yang, S.M., Rajaram, K., Hwang, S.W., 2022. Adv. Sustain. Syst. 6, 2100075.
Hannah, S., Brige, P., Ravichandran, A., Ramuz, M., 2019. ACS Omega 4, 1907–1915.
Harada, T., Fushimi, K., Kato, A., Ito, Y., Nishijima, S., Sugaya, K., Yamada, S., 2010. Biol. Pharm. Bull. 33, 653.
Hoag, N., Gani, J., 2015. Int. Neurourol. J. 19, 185–189.
Hu, H., Huang, H., Li, M., Gao, X., Yin, L., Qi, R., Wu, R.S., Chen, X., Ma, Y., Shi, K., Li, C., Maus, T.M., Huang, B., Lu, C., Lin, M., Zhou, S., Lou, Z., Gu, Y., Chen, Y., Lei, Y., Wang, X., Wang, R., Yue, W., Yang, X., Bian, Y., Mu, J., Park, G., Xiang, S., Cai, S., Corey, P.W., Wang, J., Xu, S., 2023. Nature 613, 667–675.
Huang, S., Liu, Y., Zhao, Y., Ren, Z., Guo, C.F., 2019. Adv. Funct. Mater. 29, 1805924.
Jang, T.M., Lee, J.H., Zhou, H., Joo, J., Lim, B.H., Cheng, H., Kim, S.H., Kang, I.S., Lee, K. S., Park, E., Hwang, S.W., 2020. Sci. Adv. 6, 9675–9686.
Jansen, L.E., Amer, L.D., Chen, E.Y.T., Nguyen, T.V., Saleh, L.S., Emrick, T., Liu, W.F., Bryant, S.J., Peyton, S.R., 2018. Biomacromolecules 19, 2880–2888.
Kaveti, R., Lee, J.H., Youn, J.K., Jang, T.M., Han, W.B., Yang, S.M., Shin, J.W., Ko, G.J., Kim, D.J., Han, S., Kang, H., Bandodkar, A.J., Kim, H.Y., Hwang, S.W., 2024. Adv. Mater. 36, 2307391.
Kim, B.H., Li, K., Kim, J.T., Park, Y., Jang, H., Wang, X., Xie, Z., Won, S.M., Yoon, H.J., Lee, G., Jang, W.J., Lee, K.H., Chung, T.S., Jung, Y.H., Heo, S.Y., Lee, Y., Kim, Juyun, Cai, T., Kim, Y., Prasopsukh, P., Yu, Y., Yu, X., Avila, R., Luan, H., Song, H., Zhu, F., Zhao, Y., Chen, L., Han, S.H., Kim, Jiwoong, Oh, S.J., Lee, H., Lee, C.H., Huang, Y., Chamorro, L.P., Zhang, Y., Rogers, J.A., 2021. Nature 597, 503–510.
Kim, D.H., Lu, N., Ghaffari, R., Kim, Y.S., Lee, S.P., Xu, L., Wu, J., Kim, R.H., Song, J., Liu, Z., Viventi, J., De Graff, B., Elolampi, B., Mansour, M., Slepian, M.J., Hwang, S., Moss, J.D., Won, S.M., Huang, Y., Litt, B., Rogers, J.A., 2011. Nat. Mater. 10, 316–323.
Kim, Hodam, Cha, H.S., Kim, M., Lee, Y.J., Yi, H., Lee, S.H., Ira, S., Kim, Hojoong, Im, C. H., Yeo, W.H., 2024. Adv. Sci. 11, 2305871.
Kim, T., Shin, Y., Kang, K., Kim, Kiho, Kim, G., Byeon, Y., Kim, H., Gao, Y., Lee, J.R., Son, G., Kim, Taeseong, Jun, Y., Kim, J., Lee, J., Um, S., Kwon, Y., Son, B.G., Cho, M., Sang, M., Shin, J., Kim, Kyubeen, Suh, J., Choi, H., Hong, S., Cheng, H., Kang, H.G., Hwang, D., Yu, K.J., 2022. Nat. Commun. 13, 5815.
Kim, Y., Suh, J.M., Shin, J., Liu, Y., Yeon, H., Qiao, K., Kum, H.S., Kim, C., Lee, H.E., Choi, C., Kim, H., Lee, D., Lee, J., Kang, J.H., Park, B.I., Kang, S., Kim, Jihoon, Kim, S., Perozek, J.A., Wang, K., Park, Y., Kishen, K., Kong, L., Palacios, T., Park, J., Park, M.C., Kim, H.J., Lee, Y.S., Lee, K., Bae, S.H., Kong, W., Han, J., Kim, Jeehwan, 2022. Science 377, 859–864.
Koo, J., Kim, S.B., Choi, Y.S., Xie, Z., Bandodkar, A.J., Khalifeh, J., Yan, Y., Kim, H., Pezhouh, M.K., Doty, K., Lee, G., Chen, Y.Y., Lee, S.M., D'Andrea, D., Jung, K., Lee, K.H., Li, K., Jo, S., Wang, H., Kim, J.H., Kim, J., Choi, S.G., Jang, W.J., Oh, Y.S., Park, I., Kwak, S.S., Park, J.H., Hong, D., Feng, X., Lee, C.H., Banks, A., Leal, C., Lee, H.M., Huang, Y., Franz, C.K., Ray, W.Z., MacEwan, M., Kang, S.K., Rogers, J.A., 2020. Sci. Adv. 6, eabb1093.
Koo, J., MacEwan, M.R., Kang, S.K., Won, S.M., Stephen, M., Gamble, P., Xie, Z., Yan, Y., Chen, Y.Y., Shin, J., Birenbaum, N., Chung, S., Kim, S.B., Khalifeh, J., Harburg, D.V., Bean, K., Paskett, M., Kim, J., Zohny, Z.S., Lee, S.M., Zhang, R., Luo, K., Ji, B., Banks, A., Lee, H.M., Huang, Y., Ray, W.Z., Rogers, J.A., 2018. Nat. Med. 24, 1830–1836.
Koo, J.H., Song, J.K., Kim, D.H., Son, D., 2021. ACS Mater. Lett. 3, 1528–1540.
Kwon, S., Kim, H.S., Kwon, K., Kim, H., Kim, Y.S., Lee, S.H., Kwon, Y.T., Jeong, J.W., Trotti, L.M., Duarte, A., Yeo, W.H., 2023. Sci. Adv. 9, eadg9671.
Kwon, Y.T., Kim, Y.S., Kwon, S., Mahmood, M., Lim, H.R., Park, S.W., Kang, S.O., Choi, J. J., Herbert, R., Jang, Y.C., Choa, Y.H., Yeo, W.H., 2020. Nat. Commun. 11, 3450.
Lacour, S.P., Chan, D., Wagner, S., Li, T., Suo, Z., 2006. Appl. Phys. Lett. 88, 204103.
Lee, J., Shin, S., Lee, S., Song, J., Kang, S., Han, H., Kim, Seulgee, Kim, Seunghoe, Seo, J., Kim, D., Lee, T., 2018. ACS Nano 12, 4259–4268.
Lee, J.H., Jang, T.M., Shin, J.W., Lim, B.H., Rajaram, K., Han, W.B., Ko, G.J., Yang, S.M., Han, S., Kim, D.J., Kang, H., Lim, J.H., Lee, K.S., Park, E., Hwang, S.W., 2023. ACS Nano 17, 8511–8520.
Lee, Wonryung, Kobayashi, S., Nagase, M., Jimbo, Y., Saito, I., Inoue, Y., Yambe, T., Sekino, M., Malliaras, G.G., Yokota, T., Tanaka, M., Someya, T., 2018. Sci. Adv. 4, eaau2426.
Lee, Wonho, Liu, Y., Lee, Y., Sharma, B.K., Shinde, S.M., Kim, S.D., Nan, K., Yan, Z., Han, M., Huang, Y., Zhang, Y., Ahn, J.H., Rogers, J.A., 2018. Nat. Commun. 9, 1417.
Li, Y., Li, N., Liu, W., Prominski, A., Kang, S., Dai, Y., Liu, Y., Hu, H., Wai, S., Dai, S., Cheng, Z., Su, Q., Cheng, P., Wei, C., Jin, L., Hubbell, J.A., Tian, B., Wang, S., 2023. Nat. Commun. 14, 4488.
Liu, Y., Li, J., Song, S., Kang, J., Tsao, Y., Chen, S., Mottini, V., McConnell, K., Xu, W., Zheng, Y.Q., Tok, J.B.H., George, P.M., Bao, Z., 2020. Nat. Biotechnol. 38, 1031–1036.

Maeng, J., Rihani, R.T., Javed, M., Rajput, J.S., Kim, H., Bouton, I.G., Criss, T.A., Pancrazio, J.J., Black, B.J., Ware, T.H., 2020. J. Mater. Chem. B 8, 6286–6295.
Mao, G., Schiller, D., Danninger, D., Hailegnaw, B., Hartmann, F., Stockinger, T., Drack, M., Arnold, N., Kaltenbrunner, M., 2022. Nat. Commun. 13, 1–11.
Mickle, A.D., Won, S.M., Noh, K.N., Yoon, J., Meacham, K.W., Xue, Y., McIlvried, L.A., Copits, B.A., Samineni, V.K., Crawford, K.E., Kim, D.H., Srivastava, P., Kim, B.H., Min, S., Shiuan, Y., Yun, Y., Payne, M.A., Zhang, J., Jang, H., Li, Y., Lai, H.H., Huang, Y., Park, S. Il, Gereau, R.W., Rogers, J.A., 2019. Nature 565, 361–365.
Oh, B., Lim, Y.S., Ko, K.W., Seo, H., Kim, D.J., Kong, D., You, J.M., Kim, H., Kim, T.S., Park, Seongjun, Kwon, D.S., Na, J.C., Han, W.K., Park, S.M., Park, Steve, 2023. Biosens. Bioelectron. 225, 115060.
Oh, M.H., Kim, Y.H., Lee, S.M., Hwang, G.S., Kim, K.S., Kim, Y.N., Bae, J.Y., Kim, J.Y., Lee, J.Y., Kim, Y.C., Kim, S.Y., Kang, S.K., 2023. Sci. Adv. 9, eadh9962.
Ohm, Y., Pan, C., Ford, M.J., Huang, X., Liao, J., Majidi, C., 2021. Nat. Electron. 4, 185–192.
Park, J., Choi, S., Janardhan, A.H., Lee, S.Y., Raut, S., Soares, J., Shin, K., Yang, S., Lee, C., Kang, K.W., Cho, H.R., Kim, S.J., Seo, P., Hyun, W., Jung, S., Lee, H.J., Lee, N., Choi, S.H., Sacks, M., Lu, N., Josephson, M.E., Hyeon, T., Kim, D.H., Hwang, H.J., 2016. Sci. Transl. Med. 8, 344ra86.
Riedl, C.R., Stephen, R.L., Daha, L.K., Knoll, M., Plas, E., Pflüger, H., Pflüger, P., 2000. J. Urol. 164, 2018.
Roth, G.A., Mensah, G.A., Fuster, V., 2020. J. Am. Coll. Cardiol. 76, 2980–2981.
Sekitani, T., Yokota, T., Kuribara, K., Kaltenbrunner, M., Fukushima, T., Inoue, Y., Sekino, M., Isoyama, T., Abe, Y., Onodera, H., Someya, T., 2016. Nat. Commun. 7, 11425.
Shao, L., Li, Y., Ma, Z., Bai, Y., Wang, J., Zeng, P., Gong, P., Shi, F., Ji, Z., Qiao, Y., Xu, R., Xu, J., Zhang, G., Wang, C., Ma, J., 2020. ACS Appl. Mater. Interfaces 12, 26496–26508.
Shim, J.S., Rogers, J.A., Kang, S.K., 2021. Mater. Sci. Eng. R Rep. 145, 100624.
Shin, J.W., Kim, D.J., Jang, T.M., Han, W.B., Lee, J.H., Ko, G.J., Yang, S.M., Rajaram, K., Han, S., Kang, H., Lim, J.H., Eom, C.H., Bandodkar, A.J., Hwang, S.W., 2024. Nano-Micro Lett. 16, 102.
Sim, K., Ershad, F., Zhang, Y., Yang, P., Shim, H., Rao, Z., Lu, Y., Thukral, A., Elgalad, A., Xi, Y., Tian, B., Taylor, D.A., Yu, C., 2020. Nat. Electron. 3, 775–784.
Stauffer, F., Zhang, Q., Tybrandt, K., Llerena Zambrano, B., Hengsteler, J., Stoll, A., Trüeb, C., Hagander, M., Sujata, J.M., Hoffmann, F., Schuurmans Stekhoven, J., Quack, J., Zilly, H., Goedejohann, J., Schneider, M.P., Kessler, T.M., Taylor, W.R., Küng, R., Vörös, J., 2018. Adv. Mater. Technol. 3, 1800031.
Sunwoo, S.H., Ha, K.H., Lee, S., Lu, N., Kim, D.H., 2021. Annu. Rev. Chem. Biomol. Eng. 12, 359–391.
Sunwoo, S.H., Han, S.I., Kang, H., Cho, Y.S., Jung, D., Lim, Chanhyuk, Lim, Chaehong, Cha, M. jin, Lee, S.P., Hyeon, T., Kim, D.H., 2020. Adv. Mater. Technol. 5, 1900768.
Tang, X., Shen, H., Zhao, S., Li, N., Liu, J., 2023. Nat. Electron. 6, 109–118.
Townsend, N., Kazakiewicz, D., Lucy Wright, F., Timmis, A., Huculeci, R., Torbica, A., Gale, C.P., Achenbach, S., Weidinger, F., Vardas, P., 2022. Nat. Rev. Cardiol. 19, 133–143.
Tringides, C.M., Vachicouras, N., de Lázaro, I., Wang, H., Trouillet, A., Seo, B.R., Elosegui-Artola, A., Fallegger, F., Shin, Y., Casiraghi, C., Kostarelos, K., Lacour, S.P., Mooney, D.J., 2021. Nat. Nanotechnol. 16, 1019–1029.
van Kerrebroeck, P.E.V., van Voskuilen, A.C., Heesakkers, J.P.F.A., Lycklama á Nijholt, A.A.B., Siegel, S., Jonas, U., Fowler, C.J., Fall, M., Gajewski, J.B., Hassouna, M.M., Cappellano, F., Elhilali, M.M., Milam, D.F., Das, A.K., Dijkema, H. E., van den Hombergh, U., 2007. J. Urol. 178, 2029–2034.
Viventi, J., Kim, D.H., Moss, J.D., Kim, Y.S., Blanco, J.A., Annetta, N., Hicks, A., Xiao, J., Huang, Y., Callans, D.J., Rogers, J.A., Litt, B., 2010. Sci. Transl. Med. 2, 24ra22.
Wang, F., Xue, Y., Chen, X., Zhang, P., Shan, L., Duan, Q., Xing, J., Lan, Y., Lu, B., Liu, J., 2023. Adv. Funct. Mater. 2314471.
Wang, L., Chen, K., Fan, Y., Yin, L., 2022. Med. Nov. Technol. Dev. 16, 100146.
Wang, L., Lu, C., Yang, S., Sun, P., Wang, Y., Guan, Y., Liu, S., Cheng, D., Meng, H., Wang, Q., He, J., Hou, H., Li, H., Lu, W., Zhao, Y., Wang, J., Zhu, Y., Li, Y., Luo, D., Li, T., Chen, H., Wang, S., Sheng, X., Xiong, W., Wang, X., Peng, J., Yin, L., 2020. Sci. Adv. 6, eabc6686.
Wang, S., Nie, Y., Zhu, H., Xu, Y., Cao, S., Zhang, J., Li, Y., Wang, J., Ning, X., Kong, D., 2022. Sci. Adv. 8, 5511.
Wang, S., Xu, J., Wang, W., Wang, G.J.N., Rastak, R., Molina-Lopez, F., Chung, J.W., Niu, S., Feig, V.R., Lopez, J., Lei, T., Kwon, S.K., Kim, Y., Foudeh, A.M., Ehrlich, A., Gasperini, A., Yun, Y., Murmann, B., Tok, J.B.H., Bao, Z., 2018. Nature 555, 83–88.
Xu, L., Gutbrod, S.R., Bonifas, A.P., Su, Y., Sulkin, M.S., Lu, N., Chung, H.J., Jang, K.I., Liu, Z., Ying, M., Lu, C., Webb, R.C., Kim, J.S., Laughner, J.I., Cheng, H., Liu, Y., Ameen, A., Jeong, J.W., Kim, G.T., Huang, Y., Efimov, I.R., Rogers, J.A., 2014. Nat. Commun. 5, 3329.
Xu, S., Yan, Z., Jang, K.I., Huang, W., Fu, H., Kim, J., Wei, Z., Flavin, M., McCracken, J., Wang, R., Badea, A., Liu, Y., Xiao, D., Zhou, G., Lee, J., Chung, H.U., Cheng, H., Ren, W., Banks, A., Li, X., Paik, U., Nuzzo, R.G., Huang, Y., Zhang, Y., Rogers, J.A., 2015. Science 347, 154–159.
Yan, D., Bruns, T.M., Wu, Y., Zimmerman, L.L., Stephan, C., Cameron, A.P., Yoon, E., Seymour, J.P., 2019. Adv. Healthcare Mater. 8, 1900477.
Yang, S.M., Kim, H., Ko, G.J., Choe, J.C., Lee, J.H., Rajaram, K., An, B., Han, W.B., Kim, D.J., Shin, J.W., Jang, T.M., Kang, H., Han, S., Lee, K., Oh, S.J., Hwang, S.W., 2022. Nano Today 47, 101685.
Yang, X., An, C., Liu, S., Cheng, T., Bunpetch, V., Liu, Y., Dong, S., Li, S., Zou, X., Li, T., Ouyang, H., Wu, Z., Yang, W., 2018. Adv. Healthcare Mater. 7, 1701014.
Yang, Y., Wang, J., Wang, L., Wu, Q., Ling, L., Yang, Yueying, Ning, S., Xie, Y., Cao, Q., Li, L., Liu, J., Ling, Q., Zang, J., 2022. Sci. Adv. 8, 1456.
Yin, L., Lv, J., Wang, J., 2020. Adv. Mater. Technol. 5, 2000694.
Yoshimura, N., De Groat, W.C., 1997. Int. J. Urol. 4, 111–125.
Yu, X., Xie, Z., Yu, Y., Lee, J., Vazquez-Guardado, A., Luan, H., Ruban, J., Ning, X., Akhtar, A., Li, D., Ji, B., Liu, Y., Sun, R., Cao, J., Huo, Q., Zhong, Y., Lee, C.M., Kim, S.Y., Gutruf, P., Zhang, C., Xue, Y., Guo, Q., Chempakasseril, A., Tian, P., Lu, W., Jeong, J.Y., Yu, Y.J., Cornman, J., Tan, C.S., Kim, B.H., Lee, K.H., Feng, X., Huang, Y., Rogers, J.A., 2019. Nature 575, 473–479.
Zhang, Y., Lee, G., Li, S., Hu, Z., Zhao, K., Rogers, J.A., 2023. Chem. Rev. 123, 11722–11773.
Zhou, T., Yuk, H., Hu, F., Wu, J., Tian, F., Roh, H., Shen, Z., Gu, G., Xu, J., Lu, B., Zhao, X., 2023. Nat. Mater. 22, 895–902.
Zhuang, Q., Yao, K., Wu, M., Lei, Z., Chen, F., Li, J., Mei, Q., Zhou, Y., Huang, Q., Zhao, X., Li, Y., Yu, X., Zheng, Z., 2023. Sci. Adv. 9, eadg8602.